Silver Nanoparticle-Modified Screen-Printed Carbon Electrodes for the Electrochemical Sensing of the Prostate-Specific Antigen

Yahia F. Makableh
College of Engineering and Technology, American University of the Middle East, Egaila, Kuwait
Yahia.makableh@aum.edu.kw (corresponding author)

Tamara Athamneh
Institute of Nanotechnology, Jordan University of Science and Technology, Irbid, Jordan
tkathamneh@just.edu.jo

Rama Matar
Institute of Nanotechnology, Jordan University of Science and Technology, Irbid, Jordan
ramatar21@nano.just.edu.jo

Ahmad Abu-Baker
Department of Conservation and Management of Cultural Resources, Faculty of Archaeology and Anthropology, Yarmouk University, Irbid, Jordan
ahmad.abubaker@yu.edu.jo

Sara Hijazi
Institute of Nanotechnology, Jordan University of Science and Technology, Irbid, Jordan
smhijazi20@nano.just.edu.jo

Aws Al-Qaisi
College of Engineering and Technology, American University of the Middle East, Egaila, Kuwait
Aws.Al-Qaisi@aum.edu.kw

Received: 9 July 2025 | Revised: 25 October 2025 and 24 November 2025 | Accepted: 26 November 2025

 DOI: https://doi.org/10.48084/etasr.13259

ABSTRACT

This study focuses on the development of an electrochemical aptamer-based biosensor based on silver Nanoparticle (AgNP)-modified Screen-Printed Carbon Electrodes (SPCEs) and its sensing potential against Prostate-Specific Antigen (PSA), a primary biomarker of Prostate Cancer (PCa). A significant challenge in conventional PCa screening methods is their inability to detect PSA with high sensitivity in early cancer stages. SPCEs modified with nanomaterials can overcome this limitation and revolutionize cancer diagnosis. The electrochemical behavior of the proposed biosensor was studied using voltametric and impedimetric methods. Atomic Force Microscopy (AFM) and Fourier Transform Infrared spectroscopy (FTIR) were also utilized to confirm the assembly of the sensor. The Limit of Detection (LOD) was assessed by deploying differential pulse voltammetry, where the sensor demonstrated high sensitivity and selectivity towards PSA. The LOD of the biosensor was 0.004 ng/ml, which underscores its potential as a robust tool for early PCa detection in point-of-care settings.

Keywords-aptasensor; PSA detection; electrochemical detection; silver nanoparticles

I. INTRODUCTION

Prostate Cancer (PCa) is a pressing health concern that has a global impact on the male population, and according to the World Health Organization (WHO), it is one of the most commonly diagnosed cancers in men [1]. Despite its high prevalence, the etiology of PCa remains poorly understood. However, the global occurrence and mortality rate patterns of

PCa are correlated with advancing age, with an average age of diagnosis at approximately 66 years. Besides age, the identified risk factors associated with this disease are family history, specific genetic mutations, and conditions such as Lynch syndrome [2-4]. One of the most challenging aspects of PCa is its complex symptomatology in the early stages, as asymptomatic and mild symptoms of the disease are mistaken for benign conditions or go unnoticed altogether, which further complicates the treatment regimen when the disease progresses and reaches its more advanced stages [5].

PSA is widely used as the primary biomarker for the detection and diagnosis of PCa in different populations. PSA is a 33 KDa single-chain glycoprotein secreted by the prostate gland that belongs to the family of tissue Kallikrein-related peptidases (KLKs) and is encoded by the KLK3 gene [6]. When the total PSA (tPSA) concentration in the bloodstream exceeds 4 ng/ml, it is an indicative marker for the early stage of PCa. When the concentration exceeds 10 ng/ml, it can be considered a reliable indication of the advancement of the disease [7]. Despite the advancements in understanding PSA, a significant drawback of traditional PSA-based detection is the limited specificity and inability to detect minuscule PSA concentrations. Moreover, conventional PSA tests, such as Enzyme-Linked Immunosorbent Assay (ELISA) [8], Polymerase Chain Reaction (PCR) [9], and radioimmunoassays [10], have all been employed as biomarkers to identify PCa, yet they necessitate a specialized biochemical laboratory equipped with expensive equipment and skilled personnel. More advanced techniques have been utilized for cancer detection, such as deep learning technologies [11].

Screen-Printed Electrodes (SPEs) have been used in various fields as cost-effective, easily manufactured, and robust electrochemical sensing devices. They are easy to modify with nanomaterials to enhance their surface analytical capabilities due to the increased surface-to-volume ratios [12]. Moreover, their ability to couple with biological elements makes them a promising candidate for label-free point-of-care testing [13]. Aptamer-based biosensing platforms, also known as aptasensors, have garnered considerable attention as highly selective probes. In electrochemical biosensors, the key to constructing successful aptasensors is to effectively immobilize the aptamers on the conductive electrode surface through covalent or non-covalent functionalization approaches [14].

In the realm of PSA detection, numerous studies have been conducted to test a wide variety of nanomaterials and nanocomposites with different compositions, shapes, surface morphologies, and sizes. Moreover, various biorecognition elements other than aptamers have been studied [15]. Researchers aim to achieve the highest detection sensitivity, reproducibility, ease of use, long-term stability, and detection accuracy for PCa biomarkers in point-of-care settings. Among these endeavors, authors in [16] developed a sandwich-type electrode modified with reduced Graphene Oxide (rGO) and Au Nano Particles (NPs) for the detection of fPSA and tPSA by functionalizing their respective anti-PSA antibodies. Their proposed electrochemical biosensor was characterized by AFM, Transmission Electron Microscopy (TEM), and X-Ray Diffraction (XRD), along with electrochemical techniques, such as Cyclic Voltammetry (CV) and Electrochemical Impedance Spectroscopy (EIS), as well as square wave voltammetry to measure LOD. The results were promising, exhibiting LODs of approximately 0.2 and 0.07 ng/ml for tPSA and fPSa, respectively. Authors in [17] developed an immunosensor for PSA detection using GO-modified SPCEs, assisted with ex situ prepared AgNPs as signal transducers and GO as the biofunctionalization substrate. Their proposed immunosensor has shown a detection limit of 0.27 ng/ml as well as great selectivity towards PSA in the presence of various interference. In [18], the electrochemical response of two substrates, bare Au electrodes and AuNP-modified SPCEs, against PSA using anti-PSA aptamer as the biorecognition element was investigated. The anisotropic AuNPs were grown in situ on the carbon electrodes, which allowed for higher sensitivity of the electrode compared to that of the bare Au. This is due to the formation of misaligned aptamer clusters and intermediate aptamer-PSA complexes on the electrode surface. Using EIS, the aptasensor's Charge Transfer Resistance (Rct) was obtained by changing the target PSA concentration and recording the change in the Rct. The LOD was 1.95 ng/ml, making the sensor suitable for early PCa detection. The significant impact of nanoscale materials, not only in transduction, but also in the highly effective immobilization of biorecognition molecules on their surfaces was underscored.

The purpose of this study was to construct an aptasensor using SPCEs modified with silver nanoparticles (AgNPs) and analyze the differences in electrochemical behavior for PSA detection. The key to a successful aptasensor design is the immobilization of anti-PSA ssDNA on the Working Electrode (WE) surface. AgNPs were chosen due to their ability to act as an effective transducer in electrochemical biosensing and were, therefore, functionalized with thiolated-ssDNA [19]. Electrochemical characterization techniques were employed during the aptasensor modification steps. Finally, three physiologically relevant concentrations of PSA from human semen were prepared to measure the LOD of the aptasensor and analyze its detection efficacy. The tPSA detection capacity of the aptasensor was estimated using voltametric techniques. Electrochemical tools, such as CV, and EIS, were employed along with AFM and FTIR to assess the changes at each step of the aptasensor construction.

II. EXPERIMENTAL SETUP

A. Materials

Thiol-terminated aptamer with specificity to PSA and with the sequence 5´-SH-(CH2)6-TTTTTAATTAAAGCTCGCCATCAAATAGCTTT-3′ was prepared in 1X TE buffer (10 mM Tris and 1 mM EDTA, pH 7.4). Magnesium chloride ($MgCl_2$) hexahydrate, Sodium Chloride (NaCl), PSA from human semen, Human Serum Albumin (HSA), 6-Mercapto-1-hexanol (MCH), Phosphate-Buffered Saline 1X (PBS), potassium ferrocyanide (II) trihydrate $K_4[Fe(CN)_6]\cdot 3H_2O$, and potassium hexacyanoferrate (III) $K_3[Fe(CN)_6]$ were used as received without any further purification. All aqueous solutions were prepared using nuclease-free water, unless otherwise stated.

B. Measurements and Apparatus

The SPCE DRP-110AGNP was purchased from Metrohm DropSens (Spain). The dimensions of the sensor were 33 mm × 10 mm × 0.5 mm (length × width × height). The DRP-110AGNP sensor consisted of a carbon WE modified with AgNPs, a carbon Counter Electrode (CE), and a silver Reference Electrode (RE). The sensor was washed with nuclease-free water and dried thoroughly before use. Electrochemical characterization of the constructed aptasensor was performed using an Ivium Vertex potentiostat/galvanostat (Ivium Technologies, Netherlands), where CV, Differential Pulse Voltammetry (DPV), and EIS techniques were performed and processed using Ivium Soft software. For the AgNPs-SPCE, EIS was operated in a frequency scan range from 100 kHz to 0.1 Hz and an amplitude of 0.1 V. DPV was carried out within the potential range of -0.06 to 0.5 V, a scan rate of 3 mV, and a step potential of 6 V. CV was operated in 2 cycles in the potential range of -0.6 to 0.8 V, a step potential of 1.3 mV, and a scan rate of 100 mV/s. All electrochemical measurements were carried out using 5 mM of $[Fe(CN)_6]^{-3/-4}$ as the redox mediator in a 10 mM 1X PBS solution. A Vertex 80 FTIR spectrometer (Bruker, Germany) was used to study bond formation and verify aptasensor configuration. AFM was employed to measure the surface roughness using the Scanning Probe Microscope SmartSPMTM 1000 (Novato, CA).

C. Immobilization of ssDNA Capture Probe on the Modified SPCEs

The methodology used for aptasensor preparation was adopted from [17, 20] with some modifications. The aptamers to be immobilized onto the surface of the WE were first prepared in TE buffer in an Eppendorf tube, heated gradually in a water bath at 95°C for 30 min, and then cooled down at room temperature to achieve the required aptamer structure. Subsequently, 100 µL of 5 mM $MgCl_2$ and 90 µL of 5 mM NaCl were added to each Eppendorf tube in order to reduce electrostatic repulsion within the capture probe solution and aid in the covalent functionalization of the aptamers. Before using the sensing apparatus, the sensors were washed three times with nuclease-free water and dried thoroughly and carefully. The AgNPs-SPCEs were incubated with 8 µL of the thiolated aptamer in a dark chamber under ambient temperatures for 2 h before being washed with nuclease-free water to remove unbound aptamers. Then, 8 µL of 0.1% MCH in 1X PBS was added for 2 min to block non-specific targeting sites and increase the sensitivity of the aptasensor by reducing the steric hindrance between the capture probes, and thus help with better alignment. The aptasensor was characterized at each modification step by electrochemical techniques.

D. Target Sensing Method

Three different concentrations of PSA were prepared in 1X PBS, used as target analyte, and incubated with the prepared aptasensor for 5 min under room temperature in a dark chamber. The sensors were then washed with nuclease-free water to remove unbound PSA. The sensitivity of the aptasensor was assessed using DPV, as shown in Figure 1, and the current peaks were extracted and plotted in a calibration curve to measure the LOD.

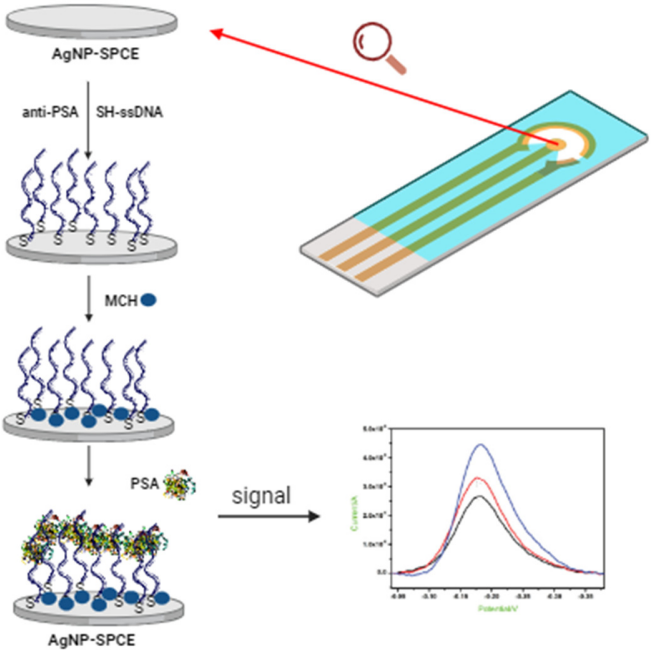

Fig. 1. Steps to modify the electrode by adding the blocking agent MCH to enhance sensitivity and a representation of the signal obtained by using DPV measurements.

III. RESULTS

A. Electrochemical Analysis

CV and EIS analysis were carried out using 5 mM of the redox mediator $[Fe(CN)_6]^{-3/-4}$ in 1X PBS, which was utilized for all electrochemical tests. Figure 2 depiucts the voltammograms for each stage of modification: pristine SPCE/AgNPs, SPCE/AgNPs/aptamer, and SPCE/AgNPs/aptamer/MCH. In theory, the alterations observed in the peak current and peak-to-peak separation within voltammograms across various stages of modification can be attributed to the electron transfer rate constant and, consequently, to the electron transfer resistance.

The anodic current decreased from 158.85 to 131.63 µA following the immobilization of the anti-PSA thiolated aptamer. Moreover, there was a significant increase in the peak-to-peak separation from 0.25 to 0.44 V. Following the introduction of the blocking agent (MCH), the anodic current increased to 145.48 µA. EIS was also employed to assess the change in the electrochemical behavior of the biosensors at each modification step, as can be seen in Figure 3, which shows the Nyquist plots of the stepwise modification behavior of the AgNPs-SPCE in order to validate the CVs of the same sensor. The semicircular response observed at higher frequencies can be attributed to the electron transfer mechanism, whereas the linear tail observed at lower frequencies can be associated with the diffusion process. In AgNPs-SPCE, a small Rct was observed with the pristine AgNPs-SPCE of around 932 Ω and increased significantly upon the immobilization of the ssDNA probe to around 1529.3 Ω, while the Rct decreased upon the addition of MCH to 1025 Ω.

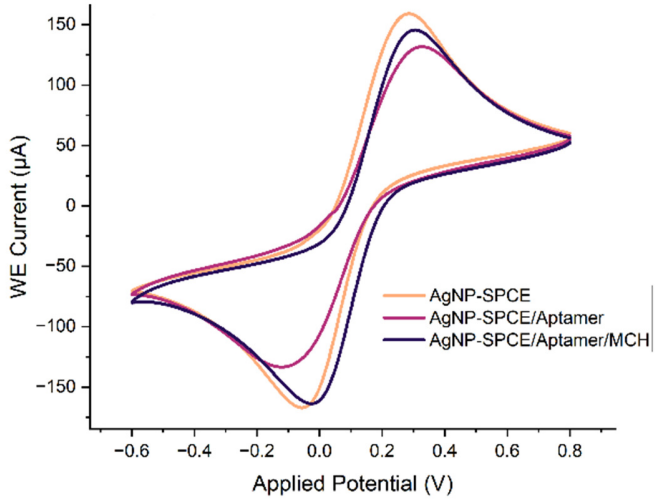

Fig. 2. CV plots of AgNPs-SPCEs after each modification step using 5 mM of the redox mediator $[Fe(CN)_6]^{-3/-4}$ in 1X PBS.

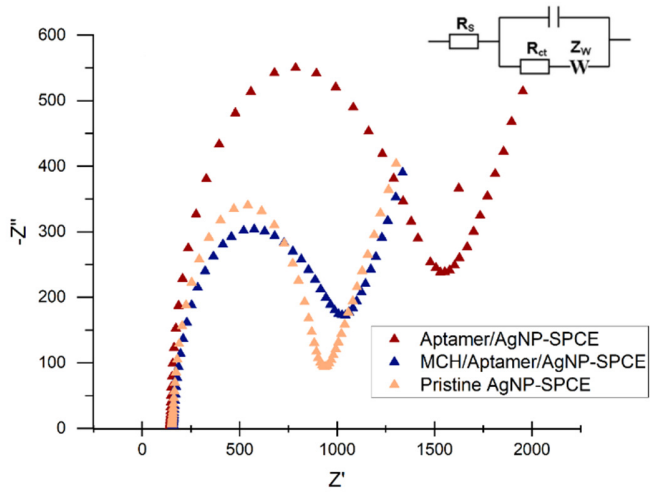

Fig. 3. Nyquist plots of AgNPs-SPCEs after each modification step using 5 mM of the redox mediator $[Fe(CN)_6]^{-3/-4}$ in 1X PBS.

In theory, the electrochemical response obtained by CV and EIS signifies the change that occurs in the electrochemical sensing system. Following the aptasensor construction steps, there was an apparent change in the peak currents in the CVs, where the peak current decreased after aptamer immobilization. This reduction in the current can be attributed to the effective formation of silver-sulfide bonds between the thiolated aptamer and Ag. The observed decrease in the anodic current signifies a modification in the electrochemical behavior of the system, as the decrease in current is caused by the adsorption of DNA aptamers, which presents a barrier to the electron transfer process. Following the addition of the blocking agent MCH, the peak increased again. This change is produced by blocking exposed sites and blocking non-targeted interactions. Furthermore, this altered current response can be explained by the enhancement in the rate of the electron transfer between the WE and the redox mediator because of the subsequent increase in the number of electroactive sites, which is attributed to the presence of MCH groups. The CV results agree with other reports in the literature discussing the electrochemical behavior of aptasensing systems [17, 20-22].

In the EIS spectra, the increase in resistance following aptamer immobilization can be attributed to the negatively charged phosphate backbone of DNA, which hinders electron transmission on the surface of the electrode. Whereas the subsequent decrease of resistance following the blocking agent addition indicates the successful removal of non-specific ssDNA probes from the surface and occupying empty sites. The EIS findings further demonstrate the successful construction of the DNA biosensor and its ability to effectively hybridize with the target ssDNA, aligning with the results obtained from CV. These results are consistent with those of [23-25].

B. AFM Analysis

AFM analysis was conducted to confirm the effectiveness of the aptasensor modification steps by measuring the changes in the average surface roughness (Ra) of the WE. Figure 4 illustrates the 3D and 2D images of: (a) the pristine AgNPs-SPCE, (b) aptamer/AgNPs-SPCE, and (c) PSA/MCH/aptamer/AgNPs-SPCE. The surface of the WE of pristine AgNP-SPCE showed a globular like structure due to the presence of AgNPs on the carbon electrode, with a Ra value of about 25.6 nm. After ssDNA immobilization, there was a change in the structure of the surface, an increase in roughness (38.8 nm), and disruption of homogeneity due to the unaligned ssDNA probes on the surface of the WE prior to the addition of MCH. After the incubation with PSA target protein, a further increase in surface roughness (52.4 nm) was observed, confirming that the capture probe successfully attached to the PSA molecules. The AFM findings agree with some reports in the literature. Among them authors in [17] developed a biosensor modified with AuNPs that exhibited an increase in Ra upon the incubation with target protein from 17.39 nm to 40.53 nm. However, in [22], the Ra value decreased from 38 to 25.2 nm after PSA incubation using a gold nanoparticle-modified SPCE. This discrepancy could be due to the varied materials used to modify the carbon electrode, as the material type influences aptamer folding and attachment to the PSA protein.

C. FTIR Spectroscopy

FTIR spectroscopy was performed in the wavenumber range of 400-4000 cm^{-1}. The changes observed in the spectra following the immobilization of the thiol anti-PSA aptamer with AgNPs are depicted in Figure 5. The peaks at approximately 1100 cm^{-1} originate from the stretching vibrations of the phosphate groups, indicating the presence of a primary sulfide group. This means that the aptamer was successfully immobilized onto the surface of the AgNPs-modified electrode. Moreover, very weak bands of alkanethiol are observed around 2600-2700 cm^{-1} related to the S-CH stretching, as well as bands in the range from 2870 – 3150 cm^{-1} that are attributed to the symmetric and asymmetric C-H vibrations. No significant changes were observed in the FTIR spectra after the addition of MCH. This indicates that the signals from the capture probe masked those of MCH owing to the similar chemical compositions, which is also consistent with [17, 22, 24].

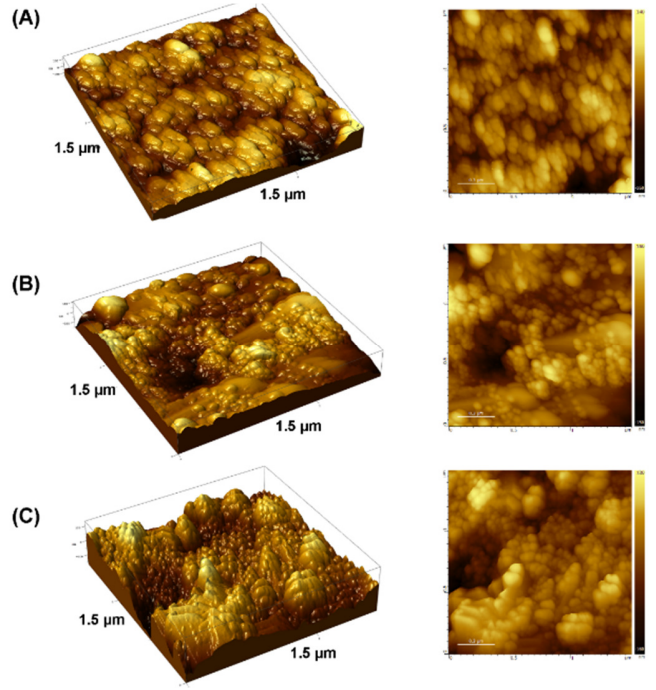

Fig. 4. AFM images of AgNPs-SPCEs after each modification step: (a) pristine AgNPs-SPCE, (b) aptamer/AgNPs-SPCE, (c) PSA/MCH/aptamer/AgNPs-SPCE.

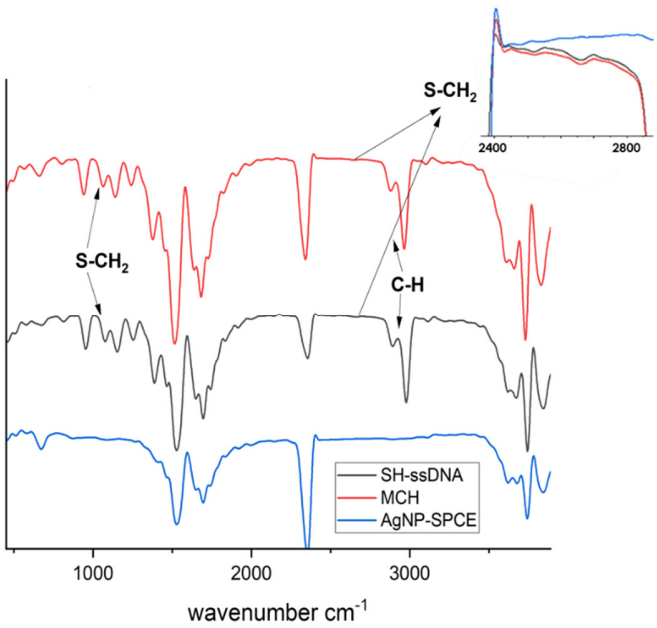

Fig. 5. FTIR spectra of AgNPs-SPCEs after each modification step.

D. Target Analyte Detection

The charging current is represented in DPV as a relatively steady baseline, allowing for greater background separation and a lower detection limit. Therefore, DPV was chosen to measure the LOD of the constructed aptasensor for detecting three different clinically relevant concentrations. The DPV analysis was carried out using 5 mM of the redox mediator $[Fe(CN)_6]^{-3/-4}$ in 1X PBS, and the results are shown in Figure 6. The current responses were plotted as a calibration curve, where the response exhibited linearity with the current increasing as the concentration of PSA decreased. Three physiologically relevant PSA concentrations (0.1, 1, and 10 ng/mL) were selected to span the clinically significant range for early cancer detection, as PSA levels exceeding 4 ng/mL are considered elevated. The calibration function of this relationship was calculated to be $I(\mu A) = -2.382 \log[PSA/M] - 7.784$, with an R^2 value of 1 (most likely due to the small analyte sample size of n =3). Then, LOD was calculated using (1) and was found to be 0.004 ng/ml:

$$LOD = 10(I - y)/(-x) \quad (1)$$

where I is the mean of three blank measurements ($\bar{x}$) + 3σ, and σ is the standard deviation. The mean and standard deviation were measured to be 10.963 and 1.976, respectively. The observed variability is consistent with the electrode-to-electrode variation in commercial SPCEs and the manual aptamer immobilization procedure, which are typical challenges in biosensor development that could be addressed through process optimization in future work.

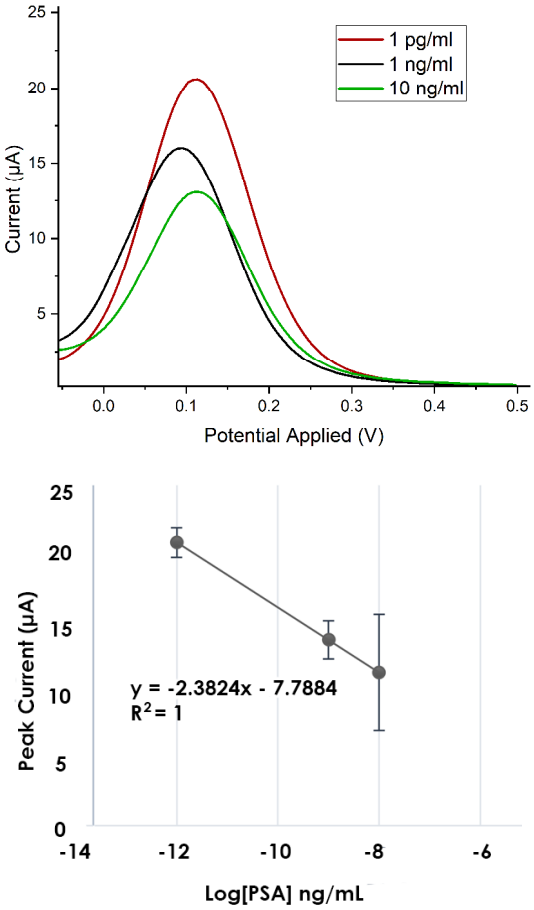

Fig. 6. DPV measurements for three concentrations of PSA in PBS performed in a 5 mM $[Fe(CN)_6]^{-3/-4}$, n = 3 in AgNPs-SPCE, and its respective calibration curve, slope = -2.382 and intercept = -7.784, $R^2 = 1$.

As shown by the DPV curves in Figure 6, the reduction in the main peak can be attributed to the complex interplay of

steric hindrance, charge interactions, and electron transfer processes. PSA's binding efficiency to the anti-PSA ssDNA is most likely hampered by steric hindrance caused by conformational changes of the ssDNA during binding. Concurrently, at the used pH of the buffer solution of (7.2 ±0.01), the net negative charge of PSA molecules causes repulsive interactions with the negatively charged aptamer, resulting in the formation of negatively charged single-stranded oligonucleotides. The interaction of charge repulsion and steric constraints affects the effectiveness of electron transfer processes and chemical reactions occurring at the electrode interface, resulting in a decrease in observed faradic current. This electrochemical response of this PSA biosensor agrees with [26, 27].

E. Selectivity and Specificity

In order to assess the ability of the aptasensor to selectively bind to PSA in the presence of interferences, a selectivity analysis was performed using DPV. HSA was chosen as a target probe to perform this analysis due to its abundance in human blood plasma. The selectivity of the aptasensor was measured against 15 ng/ml of PSA, 15 ng/ml HSA, and a mixture of 10 ng/ml PSA and 15 ng/ml HAS, as displayed in Figure 7. The current peak value of PSA was 19.6 µA, as opposed to 11.45 µA for HSA.

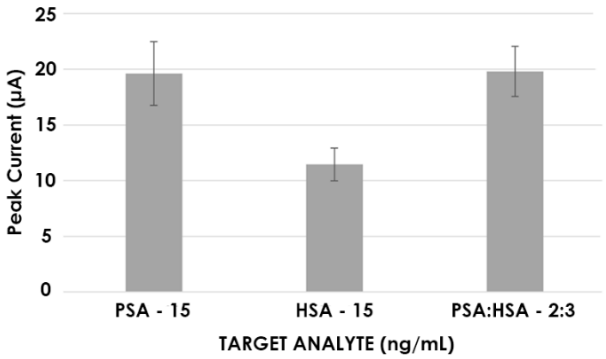

Fig. 7. Selectivity of the AgNPs-SPCE for PSA (15 ng/ml) against HSA (15 ng/ml) and PSA-HSA mixture. DPV was carried out within the potential range of -0.06 V to 0.5 V, and a scan rate of 50 mV in 5 mM of $[Fe(CN)_6]^{-3/-4}$ /10 mM 1X PBS.

Overall, the produced biosensor exhibited high sensitivity and a low LOD for PSA, making it suitable for early diagnosis and disease progression monitoring in individuals with PSA levels much lower than the cutoff value of 2.5 ng/ml. This is due to the excellent conductivity of AgNPs, which enhances electron transfer between the redox probe and WE surface. Moreover, the intrinsic size-dependent properties of AgNPs enabled them to efficiently bind to the thiolated ssDNA probe through Ag-thiol linkages, enhancing their specificity and allowing the formation of a highly aligned ssDNA layer. This indicates that employing AgNPs in this biosensor system enables it to be appropriate to measure low levels of PSA, as well as high clinically relevant levels of PSA above 4 ng/ml.

Regarding the selectivity and specificity of this sensor, as portrayed in Figure 7, the sensor showed good selectivity towards PSA. This higher current value for PSA indicates that the sensor has good selectivity towards PSA. Moreover, the mixture containing PSA had a high current value due to the contribution of the PSA protein, further confirming the ability of the sensors to distinguish the presence of PSA among interferences. In comparison, authors in [22] developed an aptasensor for PSA detection based on an electrode modified with AuNPs and Multiwalled Carbon Nanotubes (MWCNTs). The SPCE was modified with an AuNPs/MWCNTs nanocomposite to assess its ability to enhance PSA detectability with an anti-PSA aptamer as a biorecognition element and MCH, and 6-(ferrocenyl) hexanethiol (FsCH) as blocking agents. The aptasensor showed an enhanced sensitivity and extremely low detection limit of about 0.001 ng/ml when MCH was used as a blocking agent, and 5 ng/ml when FsCH was used. The response obtained with the AuNPs-MWCNTs-SPCE/ssDNA/MCH sensor was lower than that of both aptasensors presented in this study. This indicates that the synergistic effect of the unique properties of both AuNPs/MWCNTs as nanomaterials has contributed to the enhancement of the detection limit. Nevertheless, the AgNPs-SPCE aptasensor showed comparable results with the AuNPs/MWCNTs-SPCE in PSA detection of 0.004 ng/ml and through selectivity analysis. As a result, both sensors can be used to develop tools for PSA detection, with the AuNPs/MWCNTs-SPCE exhibiting a slightly more favorable potential.

IV. CONCLUSIONS

This study demonstrates the successful development of an aptasensor using silver nanoparticles (AgNPS) modified Screen Printed Carbon Electrodes (SPCEs) for the electrochemical detection of Prostate Specific Antigen (PSA). The key to successful aptasensor construction lies in the effective immobilization of the thiolated capture probe onto the AgNPs surface through stable interactions, which enables the formation of a well aligned sensing layer. The multiple characterization methods employed, including cyclic voltammetry, electrochemical impedance spectroscopy, atomic force microscopy, and Fourier Transform Infrared spectroscopy (FTIR), provided consistent evidence of successful electrode modification at each construction step, validating the robustness of the proposed methodology.

The developed AgNPs/SPCE aptasensor demonstrated high sensitivity and selectivity toward PSA detection, achieving a Limit of Detection (LOD) of 0.004 ng/mL. This sensitivity positions the sensor as a promising tool for early stage Prostate Cancer (PCa) screening, capable of detecting PSA concentrations well below the clinical cutoff value of 4 ng/mL. The selectivity of the sensor was confirmed through interference studies, demonstrating its ability to distinguish PSA from competing proteins such as human serum albumin.

The novelty of this work lies in demonstrating that commercially available AgNPs-modified SPCEs can achieve a low detection limit of 0.004 ng/mL for PSA detection through a simplified aptamer immobilization approach. Unlike previous studies that required ex-situ nanoparticle synthesis or multi-step nanocomposite preparation, such as AuNPs/ Multiwalled Carbon Nanotubes (MWCNTs) (0.001 ng/mL) or reduced Graphene Oxide (rGO)-based systems (0.2-0.27 ng/mL), the

proposed approach leverages the inherent properties of pre deposited AgNPs for direct thiol-aptamer binding, offering a cost-effective, readily scalable, and straightforward platform for point of care PCa screening without compromising sensitivity.

ACKNOWLEDGMENTS

This work was supported by the Deanship of Research of Jordan University of Science and Technology and by the Royal Hashemite Courte under the Innovative Project Funds for Nanotechnology.

REFERENCES

[1] P. Rawla, "Epidemiology of Prostate Cancer," *World Journal of Oncology*, vol. 10, no. 2, pp. 63–89, Apr. 2019, https://doi.org/10.4021/wjon.v10i2.1191.

[2] S. Ryan, M. A. Jenkins, and A. K. Win, "Risk of Prostate Cancer in Lynch Syndrome: A Systematic Review and Meta-analysis," *Cancer Epidemiology, Biomarkers & Prevention*, vol. 23, no. 3, pp. 437–449, Mar. 2014, https://doi.org/10.1158/1055-9965.EPI-13-1165.

[3] C. Messina *et al.*, "BRCA Mutations in Prostate Cancer: Prognostic and Predictive Implications," *Journal of Oncology*, vol. 2020, no. 1, 2020, Art. no. 4986365, https://doi.org/10.1155/2020/4986365.

[4] F. Bray *et al.*, "Global cancer statistics 2022: GLOBOCAN estimates of incidence and mortality worldwide for 36 cancers in 185 countries," *CA: A Cancer Journal for Clinicians*, vol. 74, no. 3, pp. 229–263, 2024, https://doi.org/10.3322/caac.21834.

[5] M. S. Litwin and H.-J. Tan, "The Diagnosis and Treatment of Prostate Cancer: A Review," *JAMA*, vol. 317, no. 24, pp. 2532–2542, June 2017, https://doi.org/10.1001/jama.2017.7248.

[6] A. Moradi, S. Srinivasan, J. Clements, and J. Batra, "Beyond the biomarker role: prostate-specific antigen (PSA) in the prostate cancer microenvironment," *Cancer and Metastasis Reviews*, vol. 38, no. 3, pp. 333–346, Sept. 2019, https://doi.org/10.1007/s10555-019-09815-3.

[7] A. W. Roddam *et al.*, "Use of Prostate-Specific Antigen (PSA) Isoforms for the Detection of Prostate Cancer in Men with a PSA Level of 2–10 ng/ml: Systematic Review and Meta-Analysis," *European Urology*, vol. 48, no. 3, pp. 386–399, Sept. 2005, https://doi.org/10.1016/j.eururo.2005.04.015.

[8] B. Acevedo *et al.*, "Development and validation of a quantitative ELISA for the measurement of PSA concentration," *Clinica Chimica Acta*, vol. 317, no. 1–2, pp. 55–63, Mar. 2002, https://doi.org/10.1016/S0009-8981(01)00749-5.

[9] K. Lind and M. Kubista, "Development and evaluation of three real-time immuno-PCR assemblages for quantification of PSA," *Journal of Immunological Methods*, vol. 304, no. 1–2, pp. 107–116, Sept. 2005, https://doi.org/10.1016/j.jim.2005.06.015.

[10] H. C. Graves, N. Wehner, and T. A. Stamey, "Ultrasensitive Radioimmunoassay of Prostate-Specific Antigen," *Clinical Chemistry*, vol. 38, no. 5, pp. 735–742, May 1992, https://doi.org/10.1093/clinchem/38.5.735.

[11] A. Naz, H. Khan, I. U. Din, A. Ali, and M. Husain, "An Efficient Optimization System for Early Breast Cancer Diagnosis based on Internet of Medical Things and Deep Learning," *Engineering, Technology & Applied Science Research*, vol. 14, no. 4, pp. 15957–15962, Aug. 2024, https://doi.org/10.48084/etasr.8080.

[12] F. Arduini *et al.*, "Electrochemical biosensors based on nanomodified screen-printed electrodes: Recent applications in clinical analysis," *TrAC Trends in Analytical Chemistry*, vol. 79, pp. 114–126, May 2016, https://doi.org/10.1016/j.trac.2016.01.032.

[13] E. Costa-Rama and M. T. Fernández-Abedul, "Paper-Based Screen-Printed Electrodes: A New Generation of Low-Cost Electroanalytical Platforms," *Biosensors*, vol. 11, no. 2, Feb. 2021, Art. no. 51, https://doi.org/10.3390/bios11020051.

[14] L. Hosseinzadeh and M. Mazloum-Ardakani, "Advances in aptasensor technology," in *Advances in Clinical Chemistry*, vol. 99, Elsevier, 2020, pp. 237–279.

[15] A. Raouafi, A. Sánchez, N. Raouafi, and R. Villalonga, "Electrochemical aptamer-based bioplatform for ultrasensitive detection of prostate specific antigen," *Sensors and Actuators B: Chemical*, vol. 297, Oct. 2019, Art. no. 126762, https://doi.org/10.1016/j.snb.2019.126762.

[16] Z. Akbari jonous, J. S. Shayeh, F. Yazdian, A. Yadegari, M. Hashemi, and M. Omidi, "An electrochemical biosensor for prostate cancer biomarker detection using graphene oxide–gold nanostructures," *Engineering in Life Sciences*, vol. 19, no. 3, pp. 206–216, 2019, https://doi.org/10.1002/elsc.201800093.

[17] T. Harahsheh, Y. F. Makableh, I. Rawashdeh, and M. Al-Fandi, "Enhanced aptasensor performance for targeted HER2 breast cancer detection by using screen-printed electrodes modified with Au nanoparticles," *Biomedical Microdevices*, vol. 23, no. 4, Sept. 2021, Art. no. 46, https://doi.org/10.1007/s10544-021-00586-9.

[18] T. T. N. Do *et al.*, "Anisotropic In Situ-Coated AuNPs on Screen-Printed Carbon Surface for Enhanced Prostate-Specific Antigen Impedimetric Aptasensor," *Journal of Electronic Materials*, vol. 46, no. 6, pp. 3542–3552, June 2017, https://doi.org/10.1007/s11664-016-5187-9.

[19] A. Ravindran, P. Chandran, and S. S. Khan, "Biofunctionalized silver nanoparticles: Advances and prospects," *Colloids and Surfaces B: Biointerfaces*, vol. 105, pp. 342–352, May 2013, https://doi.org/10.1016/j.colsurfb.2012.07.036.

[20] I. Rawashdeh, M. G. Al-Fandi, Y. Makableh, and T. Harahsha, "Developing a nano-biosensor for early detection of pancreatic cancer," *Sensor Review*, vol. 41, no. 1, pp. 93–100, Apr. 2020, https://doi.org/10.1108/SR-01-2020-0004.

[21] S. Hassani *et al.*, "A Sensitive Aptamer-Based Biosensor for Electrochemical Quantification of PSA as a Specific Diagnostic Marker of Prostate Cancer," *Journal of Pharmacy & Pharmaceutical Sciences*, vol. 23, pp. 243–258, July 2020, https://doi.org/10.18433/jpps31171.

[22] A. Alnaimi, A. Al-Hamry, Y. Makableh, A. Adiraju, and O. Kanoun, "Gold Nanoparticles-MWCNT Based Aptasensor for Early Diagnosis of Prostate Cancer," *Biosensors*, vol. 12, no. 12, Dec. 2022, Art. no. 1130, https://doi.org/10.3390/bios12121130.

[23] H. Khosropour, B. Rezaei, P. Rezaei, and A. A. Ensafi, "Ultrasensitive voltammetric and impedimetric aptasensor for diazinon pesticide detection by VS2 quantum dots-graphene nanoplatelets/carboxylated multiwalled carbon nanotubes as a new group nanocomposite for signal enrichment," *Analytica Chimica Acta*, vol. 1111, pp. 92–102, May 2020, https://doi.org/10.1016/j.aca.2020.03.047.

[24] M. Tertis, P. I. Leva, D. Bogdan, M. Suciu, F. Graur, and C. Cristea, "Impedimetric aptasensor for the label-free and selective detection of Interleukin-6 for colorectal cancer screening," *Biosensors and Bioelectronics*, vol. 137, pp. 123–132, July 2019, https://doi.org/10.1016/j.bios.2019.05.012.

[25] A. Villalonga, I. Estabiel, A. M. Pérez-Calabuig, B. Mayol, C. Parrado, and R. Villalonga, "Amperometric aptasensor with sandwich-type architecture for troponin I based on carboxyethylsilanetriol-modified graphene oxide coated electrodes," *Biosensors and Bioelectronics*, vol. 183, July 2021, Art. no. 113203, https://doi.org/10.1016/j.bios.2021.113203.

[26] L.-H. Pan, S.-H. Kuo, T.-Y. Lin, C.-W. Lin, P.-Y. Fang, and H.-W. Yang, "An electrochemical biosensor to simultaneously detect VEGF and PSA for early prostate cancer diagnosis based on graphene oxide/ssDNA/PLLA nanoparticles," *Biosensors and Bioelectronics*, vol. 89, no. Part 1, pp. 598–605, Mar. 2017, https://doi.org/10.1016/j.bios.2016.01.077.

[27] Z. Aayanifard *et al.*, "Ultra pH-sensitive detection of total and free prostate-specific antigen using electrochemical aptasensor based on reduced graphene oxide/gold nanoparticles emphasis on TiO2/carbon quantum dots as a redox probe," *Engineering in Life Sciences*, vol. 21, no. 11, pp. 739–752, 2021, https://doi.org/10.1002/elsc.202000118.